Size-dependent interband three-photon absorption properties of spherical CdTe quantum dots

2008 J. Phys.: Condens. Matter 20 025219

(http://iopscience.iop.org/0953-8984/20/2/025219)

J. Phys.: Condens. Matter **20** (2008) 025219 (6pp) doi:10.1088/0953-8984/20/02/025219

Size-dependent interband three-photon absorption properties of spherical CdTe quantum dots

Xiaobo Feng[1,2], **Guiguang Xiong**[1,2,3], **Xi Zhang**[1] and **Hongliang Jiang**[1]

[1] Department of Physics, Wuhan University, Wuhan 430072, People's Republic of China
[2] Key Laboratory of Acoustic and Photonics Material and Devices, Ministry of Education, Wuhan 430072, People's Republic of China

Received 6 August 2007, in final form 9 November 2007
Published 13 December 2007
Online at stacks.iop.org/JPhysCM/20/025219

Abstract
The degenerate three-photon absorption coefficient and cross section associated with the interband transition $1S_{3/2}(h)$–$1S(e)$ for CdTe spherical quantum dots have been calculated within the two-level model. The band structure and wavefunctions are derived from the 8×8 $k \cdot p$ Hamiltonian which takes into account the conduction–valence band coupling and the mixing of the valence states. The transition selection rules for three-photon absorption in the case of linearly polarized incident light are discussed in detail. The size-dependent three-photon absorption spectra versus incident photon energy have been obtained and analyzed.

1. Introduction

The nonlinearities of quantum dot (QD) structures have received much attention [1, 2] due to the considerable enhancement of their nonlinear response caused by quantum size effects. Recently, they have been widely used as optical switches, bio-labels, biosensors and imaging agents [3, 4]. In these applications, QDs are excited through two-photon absorption (2PA) or three-photon absorption (3PA) [5]. The saturation of 2PA and 3PA should be anticipated at high excitation intensity due to the finite number of excited states, and this is an unwanted property. Multi-photon absorption is a process wherein two or three photons which can have the same or different energies are absorbed by the medium simultaneously through virtual states to reach the excited state [6]. Compared with 2PA, longer excitation wavelengths can be used in 3PA-based applications providing deeper penetration depths in absorbing media [7, 8]. To our knowledge, the 2PA theory has been verified by a large number of experiments [9–11]. Research efforts on 3PA are much more limited. He *et al* [12, 13] reported a systematic investigation of both three-photon absorption spectra and dispersions of Kerr-type nonlinear refraction in wide gap semiconductors, and they also measured the 3PA for ZnO and ZnS nanocrystals. Lin *et al* studied one-, two-, and three-photon absorption properties for a series of Y-shaped molecules [6].

It is well known that three-dimensional (3D) semiconductor quantum dots exhibit a discrete set of energy levels due to the full confinement in all three dimensions, which leads to higher third-order nonlinear susceptibilities than for bulk materials. Additionally, the 2PA coefficient is related to the imaginary part of the third-order nonlinear susceptibilities while the 3PA coefficient is related to the imaginary part of the fifth-order nonlinear susceptibilities. Up to now, the theoretical study on 3PA in quantum confined materials has been much more limited than that of 2PA. Most of the studies are of bulk semiconductors [14, 15].

In this paper, we have deduced the expressions for the degenerate 3PA coefficient and the cross section for spherical CdTe quantum dots based on the more accurate electronic structure which is obtained in the effective-mass approximation under the well-known eight-band model, including the doubly degenerate conduction band and twofold-degenerate bands of heavy (hh), light (lh), and spin–orbit-split holes. It is more adequate because it takes into account not only the coupling between hh, lh and so holes but also the coupling of conduction and valence bands. Fedorov *et al* [16] theoretically analyzed the two-photon transition in CdS quantum dots using the parabolic energy band structure which did not include any band coupling. Actually, for relatively

[3] Author to whom any correspondence should be addressed.

narrow band gap semiconductors, the conduction band and valence bands are strongly coupled [17]. Starting from the rate of three-photon interband transition, the quantum dot size-dependent three-photon absorption coefficient and absorption cross section in CdTe quantum dots have been calculated within the two-level model, which regards the conduction band and valence bands themselves as the intermediate states.

2. Theory

2.1. Electron and hole energy levels and wavefunctions

We consider an isolated spherical CdTe quantum dot in which the electrons and holes are located in infinitely high potential wells. On the basis of the following eight Bloch functions [17]:

$$\begin{aligned}
\left|e^{+}\right\rangle &= \left|\tfrac{1}{2},\tfrac{1}{2}\right\rangle = |s\uparrow\rangle,\\
\left|hh^{+}\right\rangle &= \left|\tfrac{3}{2},\tfrac{3}{2}\right\rangle = -\mathrm{i}\sqrt{\tfrac{1}{2}}\,|(x+\mathrm{i}y)\uparrow\rangle,\\
\left|lh^{+}\right\rangle &= \left|\tfrac{3}{2},\tfrac{1}{2}\right\rangle = -\mathrm{i}\sqrt{\tfrac{1}{6}}[|(x+\mathrm{i}y)\downarrow\rangle - 2\,|z\uparrow\rangle],\\
\left|so^{+}\right\rangle &= \left|\tfrac{1}{2},\tfrac{1}{2}\right\rangle = -\mathrm{i}\sqrt{\tfrac{1}{3}}[|(x+\mathrm{i}y)\downarrow\rangle + |z\uparrow\rangle],\\
\left|e^{-}\right\rangle &= \left|\tfrac{1}{2},-\tfrac{1}{2}\right\rangle = |s\downarrow\rangle,\\
\left|hh^{-}\right\rangle &= \left|\tfrac{3}{2},-\tfrac{3}{2}\right\rangle = -\mathrm{i}\sqrt{\tfrac{1}{2}}\,|(x-\mathrm{i}y)\downarrow\rangle,\\
\left|lh^{-}\right\rangle &= \left|\tfrac{3}{2},-\tfrac{1}{2}\right\rangle = \mathrm{i}\sqrt{\tfrac{1}{6}}[|(x-\mathrm{i}y)\uparrow\rangle + 2\,|z\downarrow\rangle],\\
|so^{-}\rangle &= \left|\tfrac{1}{2},-\tfrac{1}{2}\right\rangle = \mathrm{i}\sqrt{\tfrac{1}{3}}[|(x-\mathrm{i}y)\uparrow\rangle - |z\downarrow\rangle],
\end{aligned} \tag{1}$$

the 8×8 $k\cdot p$ Hamiltonian can be written as [17, 18]

$$H_{k\cdot p} = \begin{bmatrix}
D_{\mathrm{el}} & -\sqrt{3}K_{+} & \sqrt{2}K_{z} & -K_{z} & 0 & 0 & K_{+} & \sqrt{2}K_{+}\\
-\sqrt{3}K_{-} & D_{hh} & -G_{-} & \frac{1}{\sqrt{2}}G_{-} & 0 & 0 & -\frac{1}{2}W^{*} & -\frac{1}{\sqrt{2}}W^{*}\\
\sqrt{2}K_{z} & -G_{+} & D_{lh} & R & K_{-} & -\frac{1}{2}W & 0 & \sqrt{\frac{3}{2}}G_{-}\\
-K_{z} & \frac{1}{\sqrt{2}}G_{+} & R & D_{so} & -\sqrt{2}K_{-} & \frac{1}{\sqrt{2}}W & -\sqrt{\frac{3}{2}}G_{-} & 0\\
0 & 0 & -K_{+} & -\sqrt{2}K_{+} & D_{\mathrm{el}} & -\sqrt{3}K_{-} & \sqrt{2}K_{z} & -K_{z}\\
0 & 0 & \frac{1}{2}W^{*} & \frac{1}{\sqrt{2}}W^{*} & -\sqrt{3}K_{+} & D_{hh} & -G_{+} & \frac{1}{\sqrt{2}}G_{+}\\
K_{+} & -\frac{1}{2}W^{*} & 0 & -\sqrt{\frac{3}{2}}G_{+} & \sqrt{2}K_{z} & -G_{-} & D_{lh} & R\\
\sqrt{2}K_{+} & -\frac{1}{\sqrt{2}}W^{*} & \sqrt{\frac{3}{2}}G_{+} & 0 & -K_{z} & \frac{1}{\sqrt{2}}G_{-} & R & D_{so}
\end{bmatrix}. \tag{2}$$

Here, each diagonal element is defined as

$$\begin{aligned}
D_{\mathrm{el}} &= E_{\mathrm{g}} + \frac{\alpha}{2m_0}\mathbf{P}^2,\\
D_{hh} &= D_{+},\\
D_{lh} &= D_{-},\\
D_{\pm} &= -\left(\frac{\gamma_1 \pm \gamma_2}{2m_0}\right)\mathbf{P}^2 \pm \frac{3}{2m_0}\gamma_2 P_z^2,\\
D_{so} &= -\Delta_0 - \frac{\gamma_1}{2m_0}\mathbf{P}^2.
\end{aligned} \tag{3}$$

And the off-diagonal terms are given by

$$\begin{aligned}
K_{\pm} &= -P_0\sqrt{1/6}P_{\pm}/\hbar,\\
G_{\pm} &= -\sqrt{3}\gamma_3 P_{\pm}P_z/m_0,\\
K_z &= -P_0\sqrt{1/3}P_z/\hbar,\\
W &= -\frac{\sqrt{3}}{m_0}(\bar{\gamma}P_{-}^2 + \mu P_{+}^2),\\
R &= -\frac{\sqrt{2}}{2m_0}\gamma_2(P^2 - 3P_z^2),\\
\bar{\gamma} &= \tfrac{1}{2}(\gamma_2+\gamma_3), \qquad \mu = \tfrac{1}{2}(\gamma_2-\gamma_3).
\end{aligned} \tag{4}$$

The operators in the Hamiltonian are expressed in terms of projection of the momentum operators, $P_{x,y,z} = -\mathrm{i}\hbar\nabla_{x,y,z}$, and $P_{\pm} = P_x \pm P_y$. The magnitude of the coupling between the conduction band and valence band is described usually in terms of the first-order Kane parameter $P_0 = \mathrm{i}(\hbar/m_0)\langle s|P_x|x\rangle$ or $E_{\mathrm{p}} = (2m_0/\hbar^2)P_0^2$, where E_{p} is the Kane energy. E_{g} is the band gap, and Δ_0 is the spin–orbit splitting. The parameter α takes into account the contribution of remote bands to the conduction (electron) effective mass. And contributions of remote bands to the hole effective masses are written in the terms of modified Luttinger parameters, $\gamma_1 = \gamma_1^L - E_{\mathrm{p}}/3E_{\mathrm{g}}$, $\gamma_2 = \gamma_2^L - E_{\mathrm{p}}/6E_{\mathrm{g}}$ and $\gamma_3 = \gamma_3^L - E_{\mathrm{p}}/6E_{\mathrm{g}}$.

With the approximation of effective mass, the wavefunction near the Γ point in Brillouin zone can be represented in terms of the product of the periodic Bloch functions at $k=0$ and envelope functions as follows [17, 19]:

$$\Psi(\mathbf{r}) = \sum_n U_n(\mathbf{r})F_n(\mathbf{r}), \tag{5}$$

where $U_n(\mathbf{r})$ is the Bloch function, which corresponds to eight band-edge wavefunctions in equation (1) ($n = 1, 2, 3, \ldots, 8$). $F_n(\mathbf{r})$ is the slowly varying envelope function, near the top of the valence band and the bottom of the conduction band, which can be expanded as

$$\begin{aligned}
F_n(\mathbf{r}) &= \sum_{n,L} C_{n,L}^{M} f_{n.L}^{M}\\
&= \sum_{n,L} C_{n,L}^{M} A_{n,L} j_L(k_n^L r) Y_L^M(\theta,\phi),
\end{aligned} \tag{6}$$

where $C_{n,L}^{M}$ are constants. $A_{n,L} = \sqrt{2/R^3}(1/[j_{L+1}(\mu_n^L)])$ is a normalization constant, $j_L(x)$ the spherical Bessel function, and $Y_L^M(\theta,\phi)$ the spherical harmonics. In the case of

the axial model, diagonal and off-diagonal elements in the Hamiltonian (2) present different inversion symmetries and the structures of operators (2) determine an inherent symmetry. In order to take full advantage of the aforementioned symmetry properties, the eight-component spinor wavefunctions in each Hilbert subspace will be expanded [17]. If we neglect the warping term, each subspace can be constructed with a combination of even and odd functions. The general forms of the spins or states can be given by [17]

$$\left|\Psi_{\mathrm{I}}^{M}(\mathbf{r})\right\rangle = \sum_{n}\sum_{L\geqslant|M|}\begin{pmatrix} C_{n,2L}^{M} f_{n,2L}^{M}(\mathbf{r})\left|e^{+}\right\rangle \\ C_{n,2L+1}^{M-1} f_{n,2L+1}^{M-1}(\mathbf{r})\left|hh^{+}\right\rangle \\ C_{n,2L+1}^{M} f_{n,2L+1}^{M}(\mathbf{r})\left|lh^{+}\right\rangle \\ C_{n,2L+1}^{M} f_{n,2L+1}^{M}(\mathbf{r})\left|so^{+}\right\rangle \\ C_{n,2L}^{M+1} f_{n,2L}^{M+1}(\mathbf{r})\left|e^{-}\right\rangle \\ C_{n,2L+1}^{M+2} f_{n,2L+1}^{M+2}(\mathbf{r})\left|hh^{-}\right\rangle \\ C_{n,2L+1}^{M+1} f_{n,2L+1}^{M+1}(\mathbf{r})\left|lh^{-}\right\rangle \\ C_{n,2L+1}^{M+1} f_{n,2L+1}^{M+1}(\mathbf{r})\left|so^{-}\right\rangle \end{pmatrix}, \tag{7}$$

and

$$\left|\Psi_{\Pi}^{M}(\mathbf{r})\right\rangle = \sum_{n}\sum_{L\geqslant|M|}\begin{pmatrix} C_{n,2L+1}^{M} f_{n,2L+1}^{M}(\mathbf{r})\left|e^{+}\right\rangle \\ C_{n,2L}^{M-1} f_{n,2L}^{M-1}(\mathbf{r})\left|hh^{+}\right\rangle \\ C_{n,2L}^{M} f_{n,2L}^{M}(\mathbf{r})\left|lh^{+}\right\rangle \\ C_{n,2L}^{M} f_{n,2L}^{M}(\mathbf{r})\left|so^{+}\right\rangle \\ C_{n,2L+1}^{M+1} f_{n,2L+1}^{M+1}(\mathbf{r})\left|e^{-}\right\rangle \\ C_{n,2L}^{M+2} f_{n,2L}^{M+2}(\mathbf{r})\left|hh^{-}\right\rangle \\ C_{n,2L}^{M+1} f_{n,2L}^{M+1}(\mathbf{r})\left|lh^{-}\right\rangle \\ C_{n,2L}^{M+1} f_{n,2L}^{M+1}(\mathbf{r})\left|so^{-}\right\rangle \end{pmatrix}. \tag{8}$$

Each state $|\Psi_{\mathrm{I}}^{M}(\mathbf{r})\rangle$ or $|\Psi_{\Pi}^{M}(\mathbf{r})\rangle$ differs from the usual descriptions which classify them according to their parities [17, 18]. The order of orbital quantum number L in equations (7) and (8) is determined by the off-diagonal elements in Hamiltonian (2). The combinations of the operators $P_{\pm}$ and P_z in the off-diagonal terms of the Hamiltonian, which show the conduction–valence band coupling and the valence band mixing, determine how the states must be constructed. The operators P_+ and P_- change the parity of the angular envelope function $Y_L^M(\theta,\phi)$ while P_z preserves the parity of the orbital angular momentum. In our infinitely high potential well model, states $\Psi_{\mathrm{I},\Pi}^{M}(\mathbf{r})$ should fulfill the boundary condition $\Psi_{\mathrm{I},\Pi}^{M}(\mathbf{r}) = 0$ at radius R. So $k_n^L = \mu_n^L/R$, where μ_n^L is the nth zero of the spherical Bessel function $j_L(x)$.

In order to get the energy levels in each independent M subspace, we use matrix multiplication instead of summation in equations (7) and (8). For reducing the order of the matrix, we replace the sum $\sum_{n,L}$ by $\sum_N$. The total number of N can be fixed when an appropriate convergence condition has been reached. The 8×8 matrix Hamiltonian can be expanded to $8N\times 8N$. Combining (2)–(8), a concise expression for the Schrödinger equation is written as

$$[H]_{8N\times 8N}\,[C]_{8N\times 1} = E\,[C]_{8N\times 1}\,. \tag{9}$$

Just diagonalizing the matrix $[H]_{8N\times 8N}$, eigenvalues and eigenvectors are obtained.

2.2. Calculation for interband three-photon absorption

Third-order time-dependent perturbation theory furnishes the following equation for the transition probability rate per unit volume of electrons in an initial state i going to a final state f by the simultaneous absorption of three photons, each of energy $\hbar\omega$:

$$W^{(3)} = \frac{2\pi}{\hbar}\sum_{\mathrm{i,f}}|M_{\mathrm{f,i}}|^2\delta(E_{\mathrm{f}} - E_{\mathrm{i}} - 3\hbar\omega), \tag{10}$$

where E_{i} and E_{f} represent the energies of the initial and final states respectively. Here the summation is over all possible transitions between the initial and final states. The matrix elements give the strengths of the transitions between these states:

$$M_{\mathrm{f,i}} = \sum_{m,n}\frac{H_{\mathrm{f},m}^{\mathrm{int}} H_{m,n}^{\mathrm{int}} H_{n,\mathrm{i}}^{\mathrm{int}}}{(E_m - E_n - 2\hbar\omega - \mathrm{i}\hbar\gamma)(E_n - E_{\mathrm{i}} - \hbar\omega - \mathrm{i}\hbar\gamma)}. \tag{11}$$

The sum $\sum_{m,n}$ is over intermediate states m and n. $H^{\mathrm{int}} = (e/mc)\mathbf{A}\cdot\mathbf{p}$ is used for the electron–photon interaction. $\mathbf{A} = A\mathbf{e}$ is the vector potential of the light wave with amplitude A and the polarization vector $\mathbf{e}$, and $\mathbf{p}$ is the electron momentum operator, and γ is the inverse of the lifetime in each excited state. The three-photon absorption coefficient α_3 is related to the three-photon transition probability $W^{(3)}$ by the simple expression

$$\alpha_3 = 2W^{(3)}(3\hbar\omega)N_0/I^3 \tag{12}$$

where I is the incident radiation intensity and the factor 2 accounts for electron spin degeneracy. Occasionally the nonlinear absorption is described in terms of absorption cross sections. In the case of three-photon absorption, the nonlinear cross section σ_3 is defined as

$$\sigma_3 = (\hbar\omega)^2\alpha_3/N_0. \tag{13}$$

Since the wavefunction near the Γ point in the Brillouin zone can be represented in terms of the product of the periodic Bloch functions at $k = 0$ and envelope functions in equation (5), then

$$\begin{aligned} H_{i,j}^{\mathrm{int}} &= \langle\Psi_i|H^{\mathrm{int}}|\Psi_j\rangle \\ &= \sum_{i,j}(eA/mc)\langle F_i|F_j\rangle\langle U_i|\mathbf{e}\cdot\mathbf{p}|U_j\rangle \\ &\quad + \sum_{i,j}(eA/mc)\langle U_i|U_j\rangle\langle F_i|\mathbf{e}\cdot\mathbf{p}|F_j\rangle. \end{aligned} \tag{14}$$

The second term in equation (14) is responsible for intraband optical transitions, since $\langle U_i|U_j\rangle = \delta_{ij}$. So this term can be neglected for the interband transitions.

According to our choice that the incident light with linear polarization $\mathbf{e}\parallel\hat{\mathbf{z}}$, the integration over the Bloch function results in size-independent dipole matrix elements:

$$\Pi = \langle U_i|\mathbf{e}\cdot\mathbf{p}|U_j\rangle = \frac{\mathrm{i}P}{\sqrt{3}} \times \begin{bmatrix} 0 & 0 & \sqrt{2} & -1 & 0 & 0 & 0 & 0 \\ 0 & 0 & 0 & 0 & 0 & 0 & 0 & 0 \\ -\sqrt{2} & 0 & 0 & 0 & 0 & 0 & 0 & 0 \\ 1 & 0 & 0 & 0 & 0 & 0 & 0 & 0 \\ 0 & 0 & 0 & 0 & 0 & 0 & \sqrt{2} & -1 \\ 0 & 0 & 0 & 0 & 0 & 0 & 0 & 0 \\ 0 & 0 & 0 & 0 & -\sqrt{2} & 0 & 0 & 0 \\ 0 & 0 & 0 & 0 & 1 & 0 & 0 & 0 \end{bmatrix}, \tag{15}$$

where $(\mathrm{i}P) = \hbar\langle s|\frac{\partial}{\partial x}|x\rangle$ is proportional to the Kane coupling parameter P_0. Considering the normalization condition of the envelope function, for the interband transition from the valence band to the conduction band the optical matrix element (14) can be rewritten as

$$H_{i,j}^{\mathrm{int}} = (eA/mc)\mathrm{i}P\Lambda_{e,h}(\mathrm{I},\Pi)\delta_{L_e,L_h}\delta_{M_e,M_h}, \tag{16}$$

where

$$\Lambda_{e,h}(\mathrm{I},\Pi) = \sum_{n,L\geqslant M}\left(\sqrt{\tfrac{2}{3}}C_{n,L}^{e^+}C_{n,L}^{lh^+} - \sqrt{\tfrac{1}{3}}C_{n,L}^{e^+}C_{n,L}^{so^+} + \sqrt{\tfrac{2}{3}}C_{n,L}^{e^-}C_{n,L}^{lh^-} - \sqrt{\tfrac{1}{3}}C_{n,L}^{e^-}C_{n,L}^{so^-}\right). \tag{17}$$

On the grounds established by equations (14)–(17), the corresponding selection rules for each optical transition in $\hat{\mathbf{z}}$ polarization can be precisely obtained. According to the structure of both Hilbert subspaces obtained (7), (8) and the element of the transition matrix (14)–(17), it can be seen that the only allowed transitions are those between $\Psi_i(h, L, M)$ and $\Psi_f(e, L, M)$ belonging to different subspaces I and II, i.e. in the same M subspace, (II) $lh^+ \rightarrow$ (I) e^+, (II) $so^+ \rightarrow$ (I) e^+, (II) $lh^- \rightarrow$ (I) e^-, (II) $so^- \rightarrow$ (I) e^-, (I) $lh^+ \rightarrow$ (II) e^+, (I) $so^+ \rightarrow$ (II) e^+, (I) $lh^- \rightarrow$ (II) e^-, and (I) $so^- \rightarrow$ (II) e^-. Moreover, in different M subspaces, some transitions are also permitted, as long as they have the same orbital angular quantum number L and magnetic quantum number M.

3. Numerical results and discussion

As can be seen from equations (10) and (11), the problem of three-photon absorption is conceptually simple. However, the calculation of reliable numerical values from the three-photon absorption transition probabilities is extremely difficult since it requires knowledge of the interaction Hamiltonian matrix elements among all the eigenstates of the quantum dot and summations over all the energy bands. In order to make the calculation of the absorption coefficients tractable, early workers usually made many approximations regarding the energy bands and intermediate states [20]. In our calculation, using the two-band model, in which the initial and final bands themselves served as the intermediate states [21], we calculated the three-photon absorption coefficient and cross section associated with the interband transition from the valence band to the conduction band.

The eigenenergies and eigenstates of electrons in quantum dots must be obtained first. The formulas for the energy levels and the wavefunctions of the valence and conduction bands of quantum dots near the Γ point in the Brillouin zone have been given in section 2. The following set of bulk parameters describes the energy band structure of CdTe: $E_g = 1.6069$ eV, $\Delta_0 = 0.953$ eV, $\gamma_1^L = 5.37$, $\gamma_2^L = 1.67$, $\gamma_3^L = 1.98$, $m_e = 0.091m_0$ and $E_p = 17.9$ eV. These result in $\alpha = 1.24$, $\gamma_1 = 1.66$, $\gamma_2 = -0.19$ and $\gamma_3 = 0.12$.

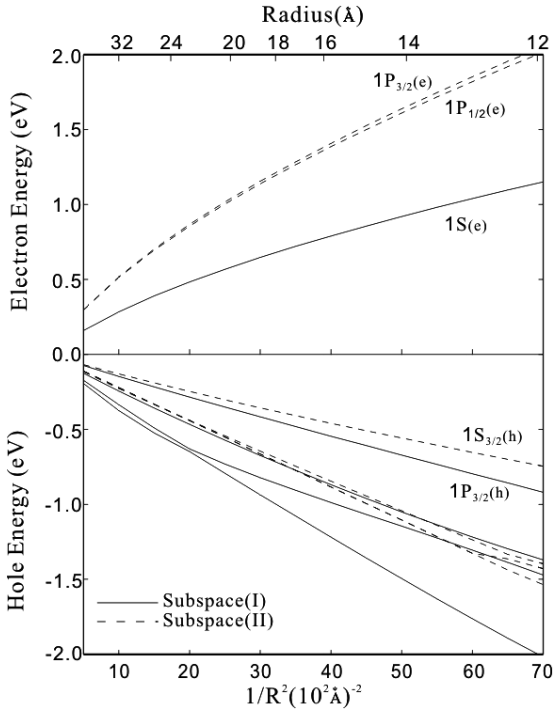

Figure 1. The energy spectra of electron and holes as a function of $1/R^2$ for the CdTe single quantum dot, coincident with [17].

In figure 1 we show the variation of the first few electron and hole energy levels as a function of $1/R^2$. It is coincident with [17]. The bottom of the conduction band and the top of the valence band are set to zero for the electron and hole respectively. It can be seen that the average spacing between levels increases with decrease of the quantum dot size due to the full confinement. We can obviously observe the existence of nonparabolicity in the conduction band levels and the effects of admixture between three holes resulting in crossing. Actually, the coupling between the conduction band and valence bands also exists, but is not strong enough to cause energy level crossing. The state for every energy level is not a 'pure' state any more. That is to say, we cannot identify them as a hh, lh or spin–orbit-split level, because each hole level is composed of one or more of these states. It is convenient to use the standard atomic notation nQ_j to describe the energy level. We only sign a few levels. It is interesting that $1P(e)$ splits into $1P_{1/2}(e)$ and $1P_{3/2}(e)$ (two) levels. The smaller the QD size, the clearer the splitting.

Using the results derived in section 2, we chose the transition from $1S_{3/2}(h)$ to $1S(e)$ to calculate the three-photon absorption coefficient and cross section if CdTe QDs are size uniform. Figures 2 and 3 demonstrate the simulated photon energy-dependent 3PA spectrum for three different size

Table 1. The three-photon absorption parameters of the CdTe quantum dots investigated.

R	E_i (eV)	E_f (eV)	$\hbar\omega$ (eV)	α_3 (cm^3/GW^2)	σ_3 (10^{-78} cm^6 s^2 photon^{-2})
1.2	−0.7454	2.7579	1.1677	0.252×10^{-4}	0.8
1.4	−0.5580	2.5261	1.0280	0.799×10^{-4}	1.9
1.6	−0.4595	2.3967	0.9521	1.551×10^{-4}	3.3

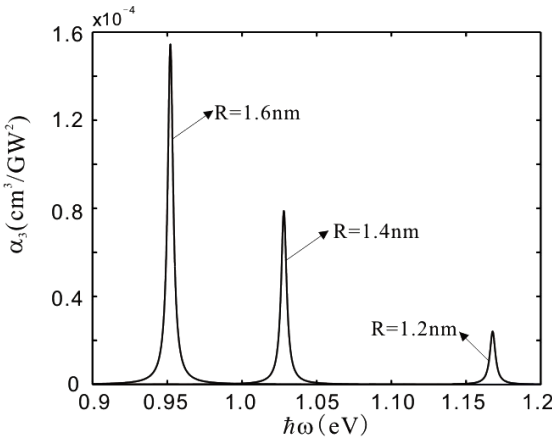

Figure 2. The three-photon absorption coefficient α_3 of different size CdTe QDs plotted as a function of incident photon energy.

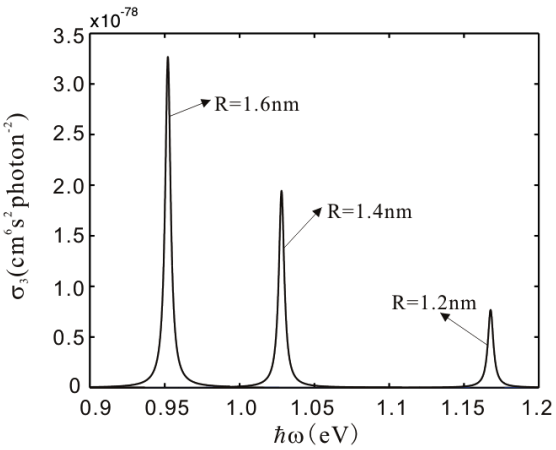

Figure 3. The three-photon absorption cross section σ_3 of different size CdTe QDs plotted as a function of incident photon energy.

quantum dots: $R = 1.2$, 1.4, 1.6 nm. It can be seen that with the increase of the QD's radius, there is a red shift for the absorption peak. This is owing to the fact that because of the consequence of the quantum size effect, energy differences between the conduction band and valence band become smaller when R increases, which can be seen obviously from figure 1. And in order to meet the occurrence condition of 3PA, the incident photon energy must satisfy $3\hbar\omega = E_f - E_i$, which is shown in equation (10) by the δ function. Also, with the increase of R, the magnitudes of the 3PA coefficient α_3 and cross section σ_3 increase too. This results from the stronger interaction between the optical field and the bigger QD. Table 1 summarizes the 3PA properties for three different size QDs. We can see that the 3PA coefficients of CdTe QDs are about 10^{-4} cm^3 GW^{-2}, and the cross sections are 10^{-78} cm^6 s^2 photon^{-2}. In order to obtain a large 3PA cross section for practical application, we should choose bigger quantum dots in the scale of the nanostructure. It is well known that the nonlinear absorption coefficients are related to the fifth-order imaginary susceptibilities by [11] $\alpha_3 = 5\pi \,\mathrm{Im}\,\chi^{(5)}/(\lambda n_0^3 c^2 \varepsilon_0^2)$, where n_0 is the linear refractive index, λ the laser wavelength, and c the speed of the light in vacuum. So we can make a numerical calculation of the imaginary susceptibilities for 3PA $\mathrm{Im}\,\chi^{(5)}(-\omega;\omega,-\omega,\omega,-\omega,\omega)$. As pointed out by Cronstrand *et al* [22], the numerical calculation of $\chi^{(5)}(-\omega;\omega,-\omega,\omega,-\omega,\omega)$ via the full SOS approach is a formidable task.

We also can obtain the intensity change for an excitation beam along the propagation direction (z axis). According to the nonlinear absorption theory, the intensity attenuation due to multi-photon absorption for the incident beam versus propagation distance has the following relationship [23]: $\mathrm{d}I(z)/\mathrm{d}z = -\alpha I(z) - \alpha_2 I^2(z) - \alpha_3 I^3(z)$, where α, α_2 and α_3 are the one-, two-,and three-photon absorption coefficients of a given medium. In the case of just a pure degenerate 3PA process occurring within the medium, the solution can be simply obtained as $I(z) = I_0/\sqrt{(1+2\alpha_3 z I_0^2)}$, where I_0 is the incident intensity of the excitation beam and z is the propagation distance within the sample medium. The experiment observation confirms that it is much harder to saturate 2PA and 3PA processes in NCs than in bulk crystal [24]. So under low intensity excitation, it is allowable to ignore the saturation. Figure 4 shows the transmitted laser beam intensity versus the incident intensity for three different size quantum dots under their own three-photon resonance absorption. It can be clearly seen that there is an optical power limiting behavior in the 3PA process. For the $R = 1.6$ nm QD, the input intensity increases from 25 to 200 GW cm^{-2} while the transmitted intensity increases from 20 to 47 GW cm^{-2}. And the bigger the QD is, the stronger the optical power limiting is, due to their larger 3PA coefficient. This means that material which has a large 3PA coefficient could be a good optical limiter.

4. Conclusions

In conclusion, within the framework of the eight-band model $k \cdot p$ effective-mass approximation we have studied the electronic structure of the CdTe quantum dot, taking into account the coupling of the doubly degenerate conduction band and the twofold-degenerate bands of heavy, light, and

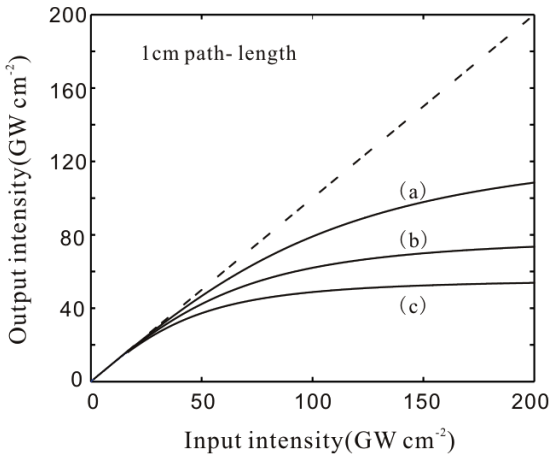

Figure 4. Transmitted intensity as a function of the incident intensity for three different size CdTe QDs under their own three-photon absorption frequency: (a) $R = 1.2$ nm, $\alpha_3 = 0.252 \times 10^{-4}$ cm^3 GW^{-2}; (b) $R = 1.4$ nm, $\alpha_3 = 0.799 \times 10^{-4}$ cm^3 GW^{-2}; (c) $R = 1.6$ nm, $\alpha_3 = 1.551 \times 10^{-4}$ cm^3 GW^{-2}.

spin–orbit-split holes. The average spacing between levels increases with decrease of the quantum dot size due to the full confinement. There can obviously be observed the existence of nonparabolicity in the conduction band levels and the effects of admixture between three holes resulting in crossing. On the basis of the energy levels and electronic states, the expressions for the size-dependent three-photon absorption coefficient and cross section have been deduced for the linear polarization of light under the two-level model, choosing the transition from $1S_{3/2}(h)$ to $1S(e)$. The numerical calculations reveal that for CdTe QDs, the magnitude of the 3PA cross sections are about 10^{-78} cm^6 s^2 photon^{-2} and, with the increase of the QD's radius, there is a red shift for the absorption peak, and the magnitudes of the 3PA coefficient α_3 and cross section σ_3 increase too. In addition, we investigate the intensity change of an excitation beam along the propagation direction according to the basic theoretical consideration of the 3PA to study the optical limiting effect. These theoretical analyses are of great importance to multi-photon fluorescence imaging and optical devices.

Acknowledgment

This work was financially supported by the National Natural Foundation of China under grant no. 10534030.

References

[1] Michalet X, Pinaud F F, Bentolila L A, Tsay J M, Doose S, Li J, Sundaresan G, Wu A, Gambhir S S and Weiss S 2005 *Science* **307** 538
[2] Gong S and Yao D 2006 *J. Phys.: Condens. Matter* **18** 10989
[3] Larson D R, Zipfel W R, Williams R M, Clark S W, Bruchez M P, Wise F W and Webb W W 2003 *Science* **300** 1434
[4] Staromlynska J, McKay T J and Wilson P 2000 *J. Appl. Phys.* **88** 1726
[5] Dubertret B, Skourides P, Norris D J, Noireaux V, Brivanlou A H and Libchaber A 2002 *Science* **298** 1759
[6] Lin N, Zhao X, Yang J, Jiang M, Liu J, Wang C, Shi W, Meng J and Weng J 2006 *J. Chem. Phys.* **124** 024704
[7] Hernandez F E, Belfield K D and Cohanoschi I 2004 *Chem. Phys. Lett.* **391** 22
[8] Hernandez F E, Belfield K D, Cohanoschi I and Schafer K J 2004 *Appl. Opt.* **43** 5394
[9] Banfi G P, Degiorgio V and Ricard D 1998 *Adv. Phys.* **47** 447
[10] Zotova I B and Ding Y J 2001 *Appl. Opt.* **40** 6654
[11] He J, Ji W, Ma G H, Tang S H, Elim H I, Sun W X, Zhang Z H and Chin W S 2004 *J. Appl. Phys.* **95** 6381
[12] He J, Qu Y, Li H, Mi J and Ji W 2005 *Opt. Express* **13** 9235
[13] He J, Ji W, Mi J, Zheng Y and Ying J Y 2006 *Appl. Phys. Lett.* **88** 181114
[14] Andrews D 1982 *J. Chem. Phys.* **77** 2831
[15] Wherrett B S 1984 *J. Opt. Soc. Am.* B **1** 67
[16] Fedorov A V, Baranov A V and Inoue K 1996 *Phys. Rev.* B **54** 8627
[17] Efros AL L and Rosen M 1998 *Phys. Rev.* B **58** 7120
[18] Prado S J, Trallero-Giner C, Alcalde A M, López-Richard V and Marques G E 2003 *Phys. Rev.* B **68** 235327
[19] Yu Y, Gao F and Xiong G 2007 *J. Phys.: Condens. Matter* **19** 236234
[20] Nathan V, Guenther A H and Mitra S S 1985 *J. Opt. Soc. Am.* B **2** 294
[21] Basov N G, Grasyuk A Z, Efimkov V F, Zubarev I G, Katulin V A and Popov J M 1966 *J. Phys. Soc. Japan. Suppl.* **21** 277
[22] Cronstrand B, Luo Y, Norman P and Ågren H 2003 *Chem. Phys. Lett.* **375** 233
[23] Lin T C, He G S, Zheng Q and Prasad P N 2006 *J. Mater. Chem.* **16** 2490
[24] He J, Mi J, Li H and Ji W 2005 *J. Chem. Phys.* B **109** 19184